Research Article | Vol. 27, No. 13 | 24 Jun 2019 | OPTICS EXPRESS 18522
Optics EXPRESS

# Carrier-to-envelope phase-stable, mid-infrared, ultrashort pulses from a hybrid parametric generator: Cr:ZnSe laser amplifier system

PAVEL KOMM,[1] UZZIEL SHEINTOP,[1,2] SALMAN NOACH,[2] AND GILAD MARCUS[1,*]

[1]*Department of Applied Physics, Faculty of Science, Hebrew University of Jerusalem, Jerusalem 9190401, Israel*
[2]*Department of Applied Physics, Electro-Optics Engineering Faculty, Jerusalem College of Technology, Jerusalem 91160, Israel*
**gilad.marcus@mail.huji.ac.il*

**Abstract:** Our Cr:ZnSe laser amplifier, seeded by parametric difference mixing, produces 72fs long pulses at the central wavelength of ~2.37μm. The stability of the carrier-to-envelope phase of the amplified seed pulses, attained at the stage of their parametric generation, is preserved through 6 orders of magnitude of laser amplification.



## 1. Introduction

Ultrashort mid-infrared (MIR) pulses are highly regarded in research areas such as molecular spectroscopy [1,2], coherent control of chemical reactions [3,4], remote sensing [5], and high filed physics. In high harmonics generation (HHG), a widely known example of high field physics, the electron is first tunnel-ionized out of a target atom in a strong optical field of a femtosecond laser pulse. The released electron then gains kinetic energy in the radiation field of the pulse. Finally, the field drives the electron back, to recollide with its parent ion. Upon recollision, its energy is converted to high frequency radiation [6]. Other possible recollision outcomes are the above threshold ionization (ATI) [7], the non-sequential double ionization (NSDI) [8] and inner shell electron excitation through inelastic re-collisions [9]. In view of the quadratic scaling law for the cut-off energy of the recolliding electron [10,11], it is straightforward to discern in what ways these processes benefit from MIR driving pulses. In HHG, for example, the additional energy of the electron translates into higher order harmonics of the fundamental [12]. For recollision excitation, it provides the opportunity to excite tightly-bound, deep-lying inner electron shells.

The carrier-to-envelope phase (CEP) of the MIR pulse can affect the outcome of the recollision to a great extent. This is especially so in the few-optical-cycle regime, where the pulse is short enough to carry only a few oscillations of the optical field. The importance of the CEP for a few-cycle pulse stems from its role in governing the relative amplitude of the field half-cycles, encompassed within its envelope. Few cycle, HHG-driving MIR pulse can spark off a single and isolated attosecond soft X-ray burst – a valuable tool for attosecond metrology. For consistent single attosecond flash production from one generating laser pulse to the next, it is imperative for them to exhibit the same CEP at the point of laser-target interaction. Such condition can only be met when the CEP of the laser pulse train is stable [13].

CEP stable MIR pulses can be derived parametrically, owing to the process of self-phase stabilization in intra-pulse difference frequency generation (DFG) [14]. For this reason, but also due to a scant coverage of the MIR spectral range by a broadband gain media, suitable for ultrafast lasers, few-cycle MIR pulses are currently produced in various optical parametric

#361126 https://doi.org/10.1364/OE.27.018522
Journal © 2019 Received 26 Feb 2019; revised 7 Jun 2019; accepted 7 Jun 2019; published 18 Jun 2019

Optics EXPRESS

amplification devices. Optical parametric amplifiers (OPAs) can have both high gain and broad gain bandwidths deep in the infrared [15–17]. However, OPAs have their drawbacks. They are prone to instabilities due to the requirement of precise spatial and temporal overlap between the pump and the signal/idler pulses in the non-linear gain medium, under stringent phase matching conditions. In addition, OPAs require expensive and complicated femtosecond/picosecond pump lasers.

The disadvantages of OPA's can be circumvented in a hybrid amplification scheme where a parametrically generated, CEP stable, femtosecond MIR pulse is amplified in a simple multi-pass laser amplifier, equipped with a suitable gain medium. Such an amplification strategy should preserve the valuable attribute of automatic CEP stabilization in parametric generation/amplification devices, while benefiting from the robustness, simplicity and energy scalability of laser amplifiers.

The laser amplifier stage of the hybrid system described here incorporates $Cr^{2+}$ doped ZnSe, as the gain element. This material belongs to the family of transition metal doped chalcogenides, several members of which exhibit very favorable spectroscopic properties for ultrashort pulses production/amplification [18]. The emission cross-section spectrum of Cr:ZnSe is more than half a micrometer broad (FWHM), is centered at $\lambda$ = 2.4μm and overlaps with the atmospheric transparency spectral window between 2 and 2.5μm. Various optical pump sources such as Tm:fiber and Er:fiber continuous-wave lasers, as well as solid state pulsed lasers: Tm:YAG, Ho:YAG/YLF and Tm:YLF (as in this case), can energize Cr:ZnSe, owing to its broad absorption band between 1.6 and 1.95μm.

Since their debut in the past decade, femtosecond MIR lasers based on Cr:ZnSe and Cr:ZnS have been evolving rapidly [19–24]. However, the practice of active CEP stabilization has not been applied to an ultrafast 2.4μm laser yet, in spite of the recognized demand for such a source. In this article, we present a combined system, composed of a passively CEP stabilized parametric seed generation followed by amplification in Cr:ZnSe multi-pass laser amplifier. It produces ultrashort pulses with carrier wavelength at approximately 2.375μm, energy of >30μJ/pulse and 72fsec pulse duration at 1kHz repetition rate. In terms of the pulse energy, the pulse duration and the pulse contrast the presented system is a major improvement of our older, previously described design [25]. More importantly, a single pulse CEP stability measurement capability of the current setup allows for the first ever CEP jitter characterization of an output of a Cr:ZnSe laser amplifier. Other implementations of a combination of parametric and laser amplification in the MIR, reaching longer carrier wavelengths [26], as well as higher energies [27], have been reported. However, in these previous reports the CEP stability of the laser-amplified output was not shown.

Optics EXPRESS

## 2. Experimental setup

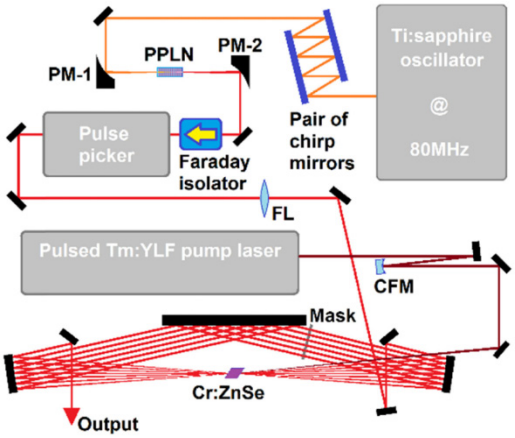


Fig. 1. The laser system architecture. The designations used here are: PPLN – periodically poled lithium niobate, PM-1(2) – parabolic mirrors, FL – $CaF_2$ focusing lens, CFM – silver coated curved focusing mirror.

A sketch of our hybrid laser system is shown in Fig. 1. To produce the CEP-stable MIR seed pulses via intrapulse DFG, we mix the spectral extremities of an ultrashort pulse from a broadband Ti:sapphire oscillator (80MHz, 6nJ/pulse, <8fs, Venteon) in a non-linear material. A typical mode-locked output spectrum of the oscillator is shown in Fig. 2(a). In this figure, the pump (blue) and the signal (red) spectral regions, that produce the MIR idler through DFG, are shown. The non-linear crystal we employ is an uncoated multi-grating periodically poled lithium niobate (PPLN), manufactured by Covesion. It has 9 gratings with poling periods ranging from 13.83 to 17.10μm. The seed is derived in two of these gratings, specifically those with $\Lambda$ = 15.1μm and $\Lambda$ = 15.6μm periodicities. To attain high conversion efficiency, the oscillator output is tightly focused into the 1mm thick PPLN, by a short focal length (15mm) silver coated parabolic mirror (marked PM-1 in Fig. 1). Upon exit, the unconverted oscillator light is recollimated back, along with the generated MIR beam, by a second parabolic mirror, identical to the first (PM-2 in Fig. 1). Prior to the entrance to the PPLN, the oscillator pulses acquire negative Group Delay Dispersion (GDD) of $-470fs^2$ at 800nm, in a pair of chirp mirrors (Venteon, DCM7). This negative GDD offsets the residual positive chirp of the pulse, accumulated before and during its propagation in the non-linear crystal.

Optics EXPRESS

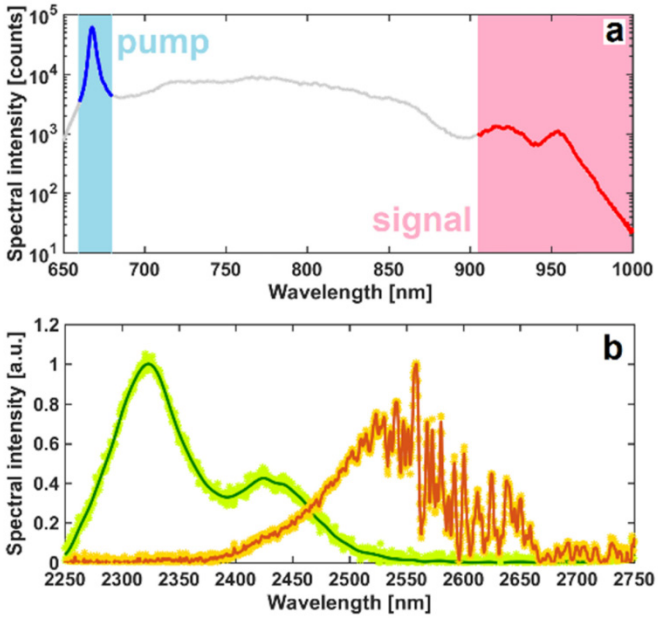


Fig. 2. (a and b). (a) – A typical output spectrum of our Ti:sapphire oscillator plotted on a logarithmic scale. The pump and the signal spectral regions are highlighted by blue and red, respectively. (b) – The measured seed spectra. The blue-shifted spectrum is obtained in the $\Lambda$ = 15.1µm grating of the PPLN crystal, while the redshifted one is derived in the grating with the 15.6µm periodicity.

Figure 2(b) shows the spectra of the parametrically generated MIR seed. To measure these, we use a 1-meter scanning monochromator and a single element PbSe photodetector covered by a MIR band-pass filter (FB2500-500, Thorlabs) which blocks the residual visible and near-infrared light from the Ti:Sapphire laser. The spectral range of our measurement is limited by the transmission window of the filter (2250nm<$\lambda$<2750nm). Of the two measured spectra shown in Fig. 2(b), the blue shifted one, peaking at 2323nm is generated in the PPLN with the $\Lambda$ = 15.1µm periodicity. The red shifted spectrum, centered at >2500nm, is produced in the $\Lambda$ = 15.6µm grating. The energy of the blue shifted seed is 50 ± 5pJ/pulse. The red shifted seed is less energetic, carrying only 40 ± 5pJ/pulse. As is evident from its spectrum, the atmospheric absorption (due to water vapor and $CO_2$) strongly reduces the spectral intensity of the generated MIR light at $\lambda$>2500nm. The bandwidths of both the red and the blue shifted seed beams are broad enough to support pulse durations of several tens of femtoseconds. Nonetheless, it is plausible to assume an even broader pre-absorption spectrum of the red shifted seed, extending further to the infrared. Its pre-absorption energy is also probably higher than 40pJ/pulse. In view of the unpurged environment of our setup, we choose the blue shifted seed for the subsequent laser amplification. Its spectrum overlaps with the atmospheric absorption region to a much lesser extent than the spectrum of the red shifted seed.

Upon its generation, the seed is steered towards the Cr:ZnSe multi-pass amplifier. To prevent feedback from the amplifier to the seed generator, we separate them by a Faraday isolator and a pulse picker (see Fig. 1). The pulse picker is based on a pair of rubidium titanyl phosphate crystals in a birefringence thermal variations compensation arrangement (Fastpulse). It reduces the rate of the seed pulses from 80MHz to 1kHz. A standard digital delay generator synchronizes between the seed pulse train and the pump laser. To further optimize the divergence angle of the MIR beam on its way to the amplifier, a positive $CaF_2$ lens (f = 25cm, marked FL in Fig. 1) is inserted in its path, at the exit from the pulse picker.

Optics EXPRESS

The Cr:ZnSe gain element of the multi-pass laser amplifier is optically pumped by a home built actively Q-switched Tm:YLF laser, which is an upgrade of an older, passively Q-switched design [28]. Here, the saturable absorber is replaced by an, acousto-optic Q-switch [29]. The pump laser provides pulses at 1kHz, with energies of 2.3mJ/pulse and central wavelength of 1886nm. At the stated energy level, its pulse duration is roughly 50ns. The pump beam is focused to a spot of 345μm (intensity FWHM) inside the Cr:ZnSe gain element by a silver coated concave mirror (f = 50cm, marked CFM in Fig. 1). To stabilize the output of the amplifier against pump variations (energy fluctuation, temporal jitter and pointing instability) the pump flux at the gain crystal is deliberately tuned high, to saturate its absorption, which is measured to be 75% (the unsaturated absorption is close to 100%).

The amplifier follows the three-mirror ring scheme originally developed by S. Backus et al. for Ti:sapphire multi-pass amplifier [30]. In our case, it is a seven-pass design based on f = 25cm silver coated concave end-mirrors and a planar gold coated side-mirror. The gain element is a single Brewster cut Cr:ZnSe crystal with $Cr^{2+}$ dopant concentration of $9.8 \cdot 10^{18} cm^{-3}$. The pump propagation distance in the crystal is 0.7cm. At the moderate absorbed pump power of 1.7W it is enough to air cool the gain medium. To mitigate the buildup of Amplified Spontaneous Emission (ASE) the amplifier includes a mask, which is an opaque aluminum plate with an array of circular holes drilled through it. The diameter of the holes is constant in each row but varies between the different rows. Such an arrangement allows us to choose the optimal hole size to sufficiently suppresses the ASE on the one hand, while inflicting tolerable losses on the amplified seed on the other. Throughout this article we present results obtained using the 1.8mm mask holes, unless otherwise stated.

## 3. Results

At the completion of seven passes, the signal beam is extracted from the amplifier and evaluated. Its energy is measured to be 40μJ/pulse. To assess the energy distribution between the amplified spontaneous emission (ASE) and the signal, we monitor the output intensity as a function of time by an extended InGaAs photodiode (Thorlabs PDA10D: 15 MHz bandwidth, ~23 ns rise time). The recorded output shows a sharp spike of the amplified seed, roughly 20ns wide, sitting atop a few hundred nanoseconds long, low ASE pedestal. Decomposing the observed waveform into the signal and the ASE contributions, we find the signal to ASE total energy ratio at 6:1. Using this ratio, we obtain a pulse energy of 34μJ (for the blue shifted seed). In term of intensity ratio between the main pulse and the ASE, if we consider a sub 100 fsec pulse duration (see below), we find a ratio of $10^7$:1. The long term energy stability of the output is tested by logging the intensity of the signal, as a function of time. We find the signal energy to be stable within 1.12% RMS (see Fig. 3).

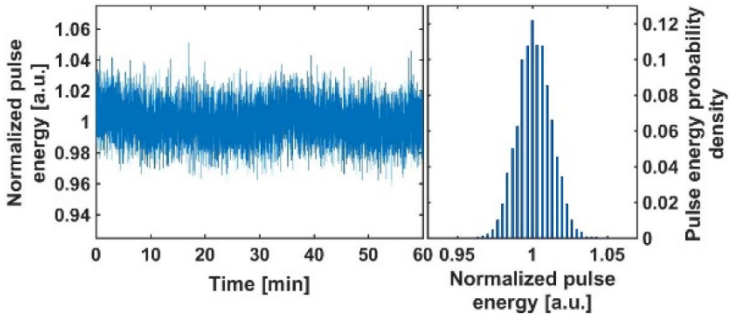


Fig. 3. Left – Temporal log of the normalized output intensity. Right – A histogramm of the scan on the left.

In order to measure the spectra of the amplified output we deploy our scanning monochromator in conjunction with the extended InGaAs photodiode. The spectral sensitivity

Optics EXPRESS

is thus limited here by the detector's responsivity cutoff at 2.6μm. Figure 4 presents the amplified blue shifted seed spectra, after 6 (green curve) and 7 (blue curve) passes in the gain medium. Evident is the gain bandwidth augmentation of the output at the seventh pass of the MIR pulse in the amplifier. The Fourier Transform Limit (FTL) of the output spectrum at the seventh pass is 43fs (FWHM) versus 73fs at the sixth pass. The blue shifted seed FTL is 59fs. Evidently, gain narrowing dictates the spectral evolution of the signal during the first 6 passes, while spectral broadening kicks-in at the final seventh pass.

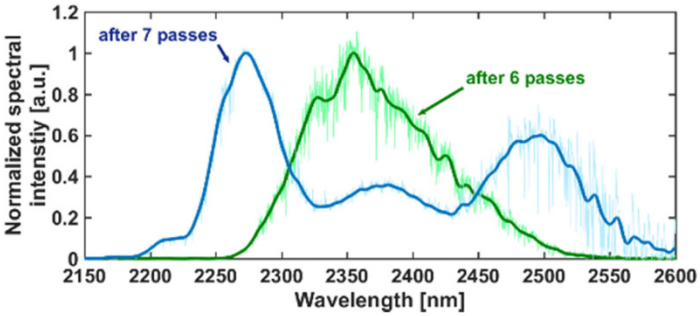


Fig. 4. The spectra of the amplified blue-shifted seed, after 6 (green curve) and 7 passes (blue curve) in the Cr:ZnSe amplifier. The thin faint lines represent the collected raw spectral data, while the thick lines are obtained by smoothing these raw graphs. What appears as noise at the long wavelengths flank of the spectra presented here, are the atmospheric absorption lines.

The phenomenon of spectral broadening accompanying laser amplification of ultrashort pulses in Cr:ZnSe and Cr:ZnS was recently reported by S. Vasilev et al [31]. They showed that considerable broadening can be attained in those cases were the peak power of the pulse reaches the critical power of self-focusing (0.4MW for ZnSe). The additional bandwidth acquired during such high peak power pulse amplification in Cr:ZnS, was shown to be as much as 65% for single pass gain value of 4.5 [32].

The observed broad spectra of the amplified pulses are only an indirect evidence of their ultrashort duration. To validate it, we use a second harmonic (SH) interferometric autocorrelator. We first convey the output through sapphire windows with various thickness, inserted at Brewster incidence to the beam. We then acquire the autocorrelation traces, as a function of the traversed sapphire length. An InGaAs photodetector sensitive up to 1.7μm is applied to measure the SH signal. The nonlinear material used for second harmonic generation (SHG) of the output is a 0.1 mm thick lithium niobate. For pulses characterized by spectra as broad as the one presented by the blue curve in Fig. 4, the bandwidth of this crystal is insufficient. The supported bandwidth is calculated by selectively computing sum-frequency coherence lengths for all possible summations of the fundamental frequencies within the laser spectrum. We consider to be phase-matched only those pairs of wavelengths, for which the calculated coherence lengths are longer than three times the physical thickness of the crystal.

To obtain trustworthy pulse duration measurements, the pump energy is lowered to 1.7mJ/pulse, to reduce the energy of the amplified signal pulse to ~20μJ. Consequently, the spectral broadening of the output is also reduced. The results are summarized in Fig. 5(a). The light blue line seen in the upper part of this figure is the normalized interferometric autocorrelation trace, acquired for traversed sapphire thickness of 18.5mm. In order to assess the pulse duration, the trace is low pass filtered, to obtain an intensity autocorrelation, which is then fitted with a Gaussian. This fit is plotted by the thick dark blue curve on top of the autocorrelation trace. The corresponding Gaussian pulse intensity envelope duration is 67fs (FWHM). The inset in Fig. 5(a) shows the output spectrum, measured along with the autocorrelation traces, its FTL is 70fs. Varying the traversed sapphire thickness nine times, from 0 to 30mm and measuring the pulse duration for each length, we obtain the plot shown

Optics EXPRESS

in Fig. 5(b). The minimum of 72 ± 16fs was found by fitting the data with a parabola. It seems, that at least in the case of limited spectral broadening, the output pulses are compressible almost down to their FTL, by a technique as simple as propagating them in a negative group velocity dispersion material, of appropriate thickness. The modulation of the autocorrelation trace, seen in Fig. 5(a), probably indicates residual higher orders of dispersion.

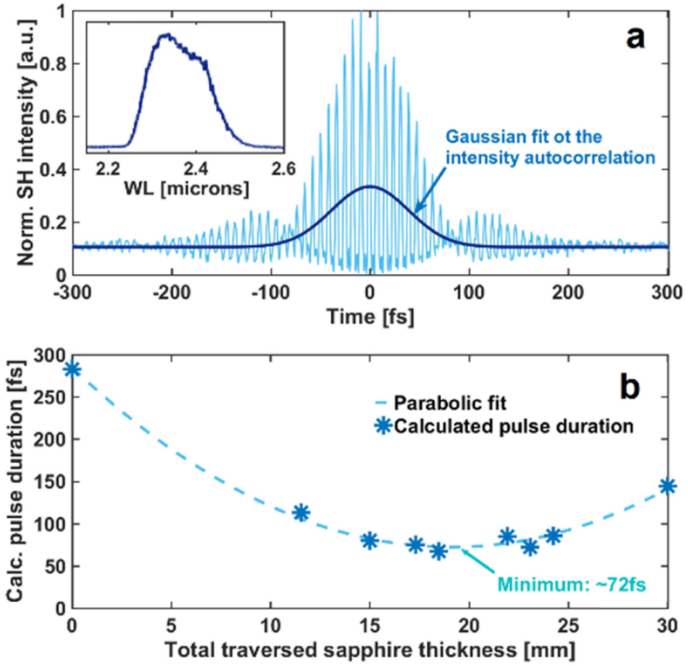


Fig. 5. (a and b). (a) – The interferometric autocorrelation of the output is traced by the light blue line. The dark blue line presents the Gaussian fit of the intensity autocorrelation, which is retrieved from the presented interferometric autocorrelation by Fourier filtering it. Shown in the inset is the output spectrum, measured alongside the autocorrelations. (b) – The Gaussian pulse durations, calculated from the interferometric autocorrelations of the output pulses, translated through sapphire plates of various thickness, are plotted against it by the dark blue asterisks. The minimum of this plot is found by a simple parabolic fit, traced by the dashed line.

To gauge the CEP stability of the amplified output we set up a simple collinear f-2f interferometer, consisting of the aforementioned 0.1mm thick lithium niobate crystal adjacent to a 5mm thick sapphire plate, with a minimal air gap between them. The beam is focused through the SHG crystal and into the sapphire by a 4mm focal length $CaF_2$ positive lens. A standard InGaAs (NIRQuest, Ocean Optics) spectrometer is used to measure the SH spectrum. Figure 6 summarizes the results. One of the measured spectra can be seen in Fig. 6(b). In order to validate that the observed interference fringes indeed stem from the CEP, we introduce a variable width $CaF_2$ wedge pair, at a Brewster angle to the beam, on its path to the f-2f interferometer. A movement of the fringes is observed as one of the wedges is translated with respect to the other, changing their combined thickness. This movement is depicted in Fig. 6(a).

Optics EXPRESS

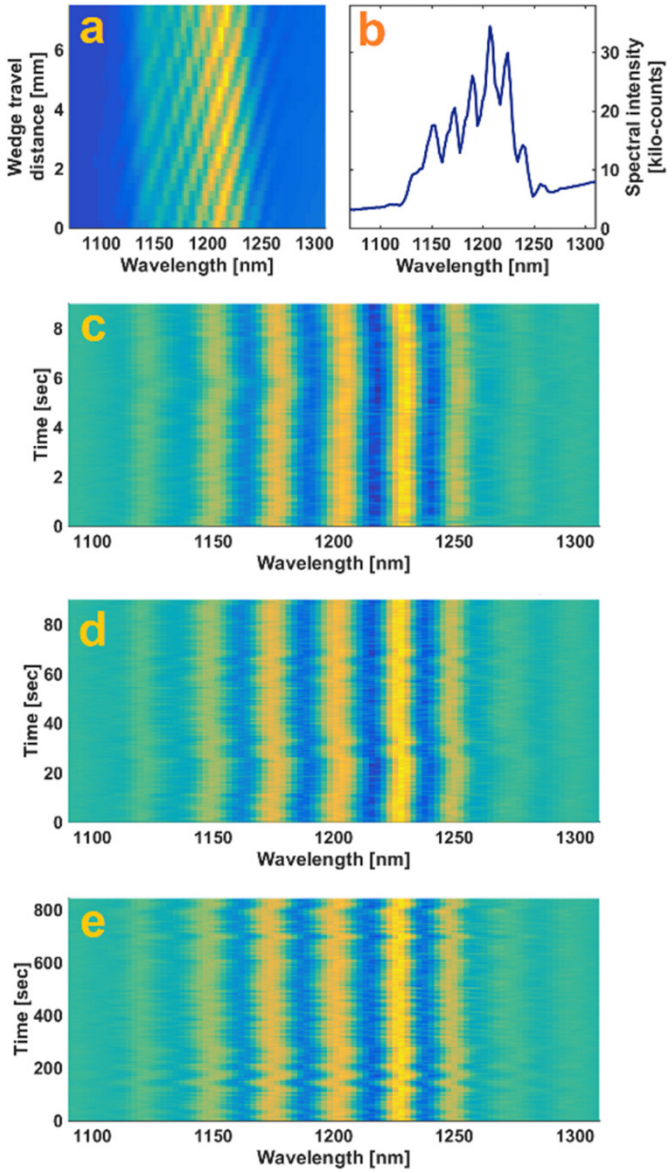


Fig. 6. (a,b,c,d and e). (a) – The shift of the fringes in the SH spectrum of the output, derived in our f-2f interferometer. This shift is caused by a change of the combined width of the two $CaF_2$ wedges, inserted at beams path, at Brewster angle. In order to change the combined width, one of the wedges is translated with respect to the other. The vertical axis of this sub-figure spans this translation. (b) – A typical SH spectrum. (c,d and e) – Fourier filtered SH spectra, as a function of time, stacked for an increasing temporal intervals: (c) – 9 seconds, (d) – 90 seconds and (e) – 14 minutes.

To construct the data set seen here the wedge is stepwise translated, taking 0.25mm steps, a total distance of 7.75mm while a spectrum of the SH is accumulated for 2min for every step taken. The sensitivity of the fringes position to the thickness of the traversed dispersive material is readily rationalized in terms of the dependence of the excess CEP, acquired by the pulse in the material, on its length. To quantify the CEP stability, we reduce the accumulation time for a single SH spectrum to sub-milliseconds. A single pulse per measurement is captured during such a brief period. We then stack 2000 of these single event spectra, for

Optics EXPRESS

three temporal intervals: 9 seconds, 90 seconds and 14 minutes. These data sets are plotted in Figs. 6(c), 6(d) and 6(e). The standard deviation of the CEP as a function of accumulation time is then evaluated to be: 250 ± 60mrad, 310 ± 60mrad and 420 ± 50mrad for the 9sec, 90sec and 14min scans respectively. These values convey a reasonable CEP stability levels of the output, on par with the values commonly reported for OPA's and amplified lasers [14,33–37]. Nevertheless, we believe that our hybrid amplifier has a capacity for a better CEP stability. For instance, installing a simple enclosure around the setup can reduce phase fluctuations by minimizing air flow.

To complete the characterization of the output, its far-field beam profile is measured. A home built scanning profiler is used for this purpose. The device consists of the PDA10D extended InGaAs photodetector capped by a pinhole with a diameter of 50um. The detector and the pinhole are translated together in a plane perpendicular to the propagation axis of the MIR beam, recording its intensity profile as a function of the spatial coordinates spanning this plane. The results are shown in Fig. 7.

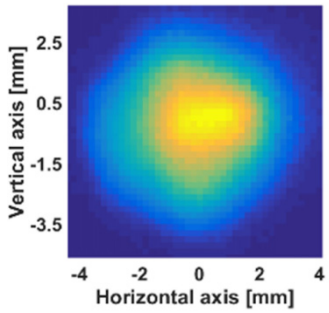


Fig. 7. The profile scan of the output beam amplified through the 1.8mm diameter holes of the amplifier mask.

## 4. Conclusion

Our hybrid amplification system presently yields few tens of μJ mid-IR CEP stable pulses, with central wavelength at 2.35-2.4μm. Their duration is measured to be around 70fs. The stability of the CEP, anchored at the stage of the parametric derivation of the MIR seed, is faithfully carried through six orders of magnitude of its amplification, in a 7-pass Cr:ZnSe laser amplifier. Additional laser amplification of the output pulses should present no difficulties, at the attained 6:1 signal to ASE total energy ratio. If we calculate the ratio of instantaneous power between the signal and the ASE, while considering the sub 100fs duration of the signal pulse, we obtain a much more reassuring figure of ~$10^7$:1. This ratio could be further improved if we chirped our pulse and further amplify it, thus extracting more energy into the pulse and reduce energy that goes to the ASE. Having in mind the current state of availability of broadband Ti:sapphire oscillators, the proposed hybrid amplification system is a simple and low-cost alternative for both actively CEP stabilized MIR lasers and OPA's.

## Funding

Israeli Ministry of Science, Technology, and Space (53998); Wolfson Foundation.

## References

1. J. Herbst, K. Heyne, and R. Diller, "Femtosecond Infrared Spectroscopy of Bacteriorhodopsin Chromophore Isomerization," Science **297**(5582), 822–825 (2002).
2. B. Bernhardt, E. Sorokin, P. Jacquet, R. Thon, T. Becker, I. T. Sorokina, N. Picqué, and T. W. Hänsch, "Mid-infrared dual-comb spectroscopy with 2.4 μm $Cr^{2+}$:ZnSe femtosecond lasers," Appl. Phys. B **100**(1), 3–8 (2010).
3. G. Marcus, L. Friedland, and A. Zigler, "Autoresonant excitation and control of molecular degrees of freedom in three dimensions," Phys. Rev. A **72**(3), 033404 (2005).

Optics EXPRESS


4. G. Marcus, A. Zigler, and L. Friedland, "Molecular vibrational ladder climbing using a sub-nanosecond chirped laser pulse," EPL **74**(1), 43–48 (2006).
5. V. V. Alexander, Z. Shi, M. N. Islam, K. Ke, G. Kalinchenko, M. J. Freeman, A. Ifarraguerri, J. Meola, A. Absi, J. Leonard, J. A. Zadnik, A. S. Szalkowski, and G. J. Boer, "Field trial of active remote sensing using a high-power short-wave infrared supercontinuum laser," Appl. Opt. **52**(27), 6813–6823 (2013).
6. F. Krausz and M. Ivanov, "Attosecond physics," Rev. Mod. Phys. **81**(1), 163–234 (2009).
7. D. B. Milošević, G. G. Paulus, D. Bauer, and W. Becker, "Above-threshold ionization by few-cycle pulses," J. Phys. B **39**(14), R203–R262 (2006).
8. B. Bergues, M. Kübel, N. G. Johnson, B. Fischer, N. Camus, K. J. Betsch, O. Herrwerth, A. Senftleben, A. M. Sayler, T. Rathje, T. Pfeifer, I. Ben-Itzhak, R. R. Jones, G. G. Paulus, F. Krausz, R. Moshammer, J. Ullrich, and M. F. Kling, "Attosecond tracing of correlated electron-emission in non-sequential double ionization," Nat. Commun. **3**(1), 813 (2012).
9. Y. Deng, Z. Zeng, Z. Jia, P. Komm, Y. Zheng, X. Ge, R. Li, and G. Marcus, "Ultrafast Excitation of an Inner-Shell Electron by Laser-Induced Electron Recollision," Phys. Rev. Lett. **116**(7), 073901 (2016).
10. M. Lewenstein, P. Balcou, M. Y. Ivanov, A. L'Huillier, and P. B. Corkum, "Theory of high-harmonic generation by low-frequency laser fields," Phys. Rev. A **49**(3), 2117–2132 (1994).
11. J. Tate, T. Auguste, H. G. Muller, P. Salières, P. Agostini, and L. F. DiMauro, "Scaling of Wave-Packet Dynamics in an Intense Midinfrared Field," Phys. Rev. Lett. **98**(1), 013901 (2007).
12. G. Marcus, W. Helml, X. Gu, Y. Deng, R. Hartmann, T. Kobayashi, L. Strueder, R. Kienberger, and F. Krausz, "Subfemtosecond K-Shell Excitation with a Few-Cycle Infrared Laser Field," Phys. Rev. Lett. **108**(2), 023201 (2012).
13. M. Hentschel, R. Kienberger, C. Spielmann, G. A. Reider, N. Milosevic, T. Brabec, P. Corkum, U. Heinzmann, M. Drescher, and F. Krausz, "Attosecond metrology," Nature **414**(6863), 509–513 (2001).
14. G. Cerullo, A. Baltuška, O. Mücke, and C. Vozzi, "Few-optical-cycle light pulses with passive carrier-envelope phase stabilization," Laser Photonics Rev. **5**(3), 323–351 (2011).
15. G. Marcus, A. Zigler, A. Englander, M. Katz, and Y. Ehrlich, "Generation of ultrawide-band chirped sources in the infrared through parametric interactions in periodically poled crystals," Appl. Phys. Lett. **82**(2), 164–166 (2003).
16. G. Marcus, A. Zigler, D. Eger, A. Bruner, and A. Englander, "Generation of a high-energy ultrawideband chirped source in periodically poled LiTaO3," J. Opt. Soc. Am. B **22**(3), 620–622 (2005).
17. X. Gu, G. Marcus, Y. Deng, T. Metzger, C. Teisset, N. Ishii, T. Fuji, A. Baltuska, R. Butkus, V. Pervak, H. Ishizuki, T. Taira, T. Kobayashi, R. Kienberger, and F. Krausz, "Generation of carrier-envelope-phase-stable 2-cycle 740-µJ pulses at 2.1-µm carrier wavelength," Opt. Express **17**(1), 62–69 (2009).
18. I. T. Sorokina and E. Sorokin, "Femtosecond $Cr^{2+}$-Based Lasers," IEEE J. Sel. Top. Quantum Electron. **21**(1), 1601519 (2015).
19. I. T. Sorokina, E. Sorokin, and T. Carrig, "Femtosecond Pulse Generation from a SESAM Mode-Locked Cr:ZnSe Laser," in *Proceedings Conference on Lasers and Electro-Optics/Quantum Electronics and Laser Science Conference and Photonic Applications Systems Technologies, Technical Digest (CD)* (Optical Society of America, 2006), paper CMQ2.
20. M. N. Cizmeciyan, J. W. Kim, S. Bae, B. H. Hong, F. Rotermund, and A. Sennaroglu, "Graphene mode-locked femtosecond Cr:ZnSe laser at 2500 nm," Opt. Lett. **38**(3), 341–343 (2013).
21. N. Tolstik, E. Sorokin, and I. T. Sorokina, "Kerr-lens mode-locked Cr:ZnS laser," Opt. Lett. **38**(3), 299–301 (2013).
22. S. B. Mirov, V. V. Fedorov, D. Martyshkin, I. S. Moskalev, M. Mirov, and S. Vasilyev, "Progress in Mid-IR Lasers Based on Cr and Fe-Doped II–VI Chalcogenides," IEEE J. Sel. Top. Quantum Electron. **21**(1), 292–310 (2015).
23. Y. Wang, T. T. Fernandez, N. Coluccelli, A. Gambetta, P. Laporta, and G. Galzerano, "47-fs Kerr-lens mode-locked Cr:ZnSe laser with high spectral purity," Opt. Express **25**(21), 25193–25200 (2017).
24. S. Vasilyev, I. Moskalev, V. Smolski, J. Peppers, M. Mirov, V. Fedorov, D. Martyshkin, S. Mirov, and V. Gapontsev, "Octave-spanning Cr:ZnS femtosecond laser with intrinsic nonlinear interferometry," Optica **6**(2), 126–127 (2019).
25. P. Komm, U. Sheintop, S. Noach, and G. Marcus, "87 fs CEP-stable Cr:ZnSe laser system," Laser Phys. **28**(2), 025301 (2018).
26. F. Potemkin, E. Migal, A. Pushkin, A. Sirotkin, V. Kozlovsky, Yu. Korostelin, Yu. Podmar'kov, V. Firsov, M. Frolov, and V. Gordienko, "Mid-IR (4–5 µm) femtosecond multipass amplification of optical parametric seed pulse up to gigawatt level in $Fe^{2+}$:ZnSe with optical pumping by a solid-state 3µm laser," Laser Phys. Lett. **13**(12), 125403 (2016).
27. X. Ren, L. H. Mach, Y. Yin, Y. Wang, and Z. Chang, "Generation of 1 kHz, 2.3 mJ, 88 fs, 2.5 µm pulses from a $Cr^{2+}$:ZnSe chirped pulse amplifier," Opt. Lett. **43**(14), 3381–3384 (2018).
28. A. Korenfeld, D. Sebbag, U. Ben-Ami, E. Shalom, G. Marcus, and S. Noach, "High pulse energy passive Q-switching of a diode-pumped Tm:YLF laser by Cr:ZnSe," Laser Phys. Lett. **12**(4), 045804 (2015).
29. U. Sheintop, E. Perez, D. Sebbag, P. Komm, G. Marcus, and S. Noach, "Actively Q-switched tunable narrow bandwidth milli-Joule level Tm:YLF laser," Opt. Express **26**(17), 22135–22143 (2018).
30. S. Backus, J. Peatross, C. P. Huang, M. M. Murnane, and H. C. Kapteyn, "Ti:sapphire amplifier producing millijoule-level, 21-fs pulses at 1 kHz," Opt. Lett. **20**(19), 2000–2002 (1995).

Optics EXPRESS


31. S. Vasilyev, I. Moskalev, M. Mirov, S. Mirov, and V. Gapontsev, "Multi-Watt mid-IR femtosecond polycrystalline $Cr(^{2+})$:ZnS and $Cr(^{2+})$:ZnSe laser amplifiers with the spectrum spanning 2.0-2.6 µm," Opt. Express **24**(2), 1616–1623 (2016).
32. S. Vasilyev, I. Moskalev, M. Mirov, V. Smolski, S. Mirov, and V. Gapontsev, "Ultrafast middle-IR lasers and amplifiers based on polycrystalline Cr:ZnS and Cr:ZnSe," Opt. Mater. Express **7**(7), 2636–2650 (2017).
33. A. Thai, M. Hemmer, P. K. Bates, O. Chalus, and J. Biegert, "Sub-250-mrad, passively carrier-envelope-phase-stable mid-infrared OPCPA source at high repetition rate," Opt. Lett. **36**(19), 3918–3920 (2011).
34. C. Li, D. Wang, L. Song, J. Liu, P. Liu, C. Xu, Y. Leng, R. Li, and Z. Xu, "Generation of carrier-envelope phase stabilized intense 1.5 cycle pulses at 1.75 µm," Opt. Express **19**(7), 6783–6789 (2011).
35. B. Langdon, J. Garlick, X. Ren, D. J. Wilson, A. M. Summers, S. Zigo, M. F. Kling, S. Lei, C. G. Elles, E. Wells, E. D. Poliakoff, K. D. Carnes, V. Kumarappan, I. Ben-Itzhak, and C. A. Trallero-Herrero, "Carrier-envelope-phase stabilized terawatt class laser at 1 kHz with a wavelength tunable option," Opt. Express **23**(4), 4563–4572 (2015).
36. R. Budriūnas, T. Stanislauskas, and A. Varanavičius, "Passively CEP-stabilized frontend for few cycle terawatt OPCPA system," J. Opt. **17**(9), 094008 (2015).
37. M. Neuhaus, H. Fuest, M. Seeger, J. Schötz, M. Trubetskov, P. Russbueldt, H. D. Hoffmann, E. Riedle, Z. Major, V. Pervak, M. F. Kling, and P. Wnuk, "10 W CEP-stable few-cycle source at 2 µm with 100 kHz repetition rate," Opt. Express **26**(13), 16074–16085 (2018).